SUMMARY OF EXPERIMENTAL RESULTS FROM M.I.T. DETECTOR ON IMP-1

STANISLAW OLBERT

Dept. of Physics, Massachusetts Institute of Technology, Cambridge, Mass., U.S.A.

This paper is an extended version of the summary of experimental results reported by Dr. Pai and myself at the AGU meeting of April 1967, in Washington, D.C. The results pertain primarily to the M.I.T. data from IMP-1, launched in November 1963.* Figure 1, taken from NESS (1966), shows the first 30 orbits of IMP-1 projected into the ecliptic plane. Apogee is at about 30 earth radii, and the major axis of the first orbit points roughly toward the sun. The orbital period is about four days so that during each revolution the major axis of the orbit rotates by about 4° toward the dawn side of the earth. In a time span of about four months, the satellite explores a vast region that covers the noon, morning, dawn, and predawn portion of the magnetosphere in the neighborhood of the ecliptic plane. Furthermore, and this is essential to the discussion, the large apogee makes it possible for the satellite not only to cross the sunward portion of the magnetosphere and the magnetosheath, but also to enter fairly deeply into the interplanetary domain where the presence of earth's magnetic field is not felt.

The region of primary interest here is the magnetosheath (also called 'the transition region' in the past). This is the region bounded by the magnetopause and the bow shock. IMP-1 was well located for this study because it scanned the dawn quadrant of the magnetosheath in a systematic way. During a period of about 80 days from the day of launch, we were able to gather an uninterrupted record of data that shows clearly, for each crossing of the bow shock and the magnetopause, how distinct and non-uniform the plasma behavior is in the magnetosheath, in comparison to other regions. The quantity of data enabled us to form large-scale averages of the measured macroscopic plasma variables, such as the density, the stream velocity, temperature, etc., and thereby test various theoretical models of 'collisionless' plasma shocks, the fluid properties of the plasma, etc.

In order to appreciate how dramatic a change the interplanetary plasma undergoes behind the bow shock, we shall briefly review the prevailing characteristics of the solar wind ahead of the bow shock. Before presenting the summary of the physical quantities pertaining to this regime, one sample of the actual measurements will be discussed. The data sample shown in Figure 2 was obtained from an M.I.T. 'Faraday cup', that is practically identical in construction to the detector used on IMP-2 and described earlier in this monograph by Dr. J. Binsack. The manner of operation of the detector will not be discussed, therefore, and we turn our attention directly to the

* The co-authors of this experiment and its analysis are: H. S. Bridge, A. Egidi, E. F. Lyon, G. Moreno, S. Olbert, and L. G. Pai.

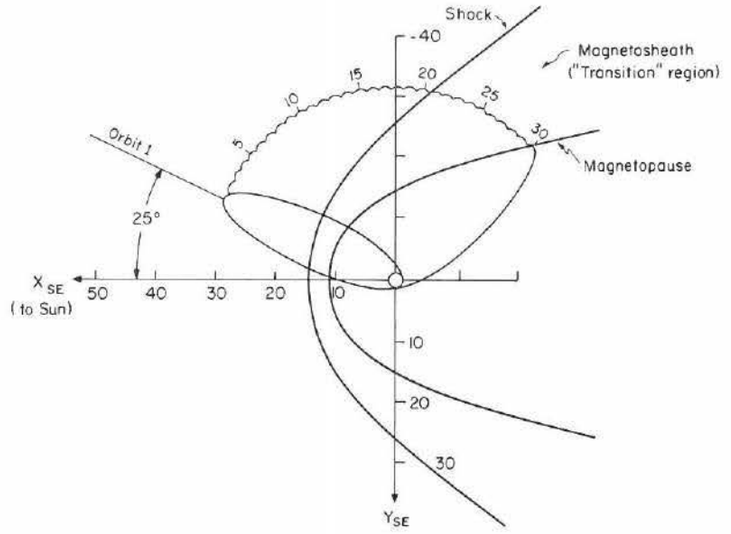

Fig. 1. Ecliptic plane projection of the first 30 orbits of IMP-1. The distances indicated on the X_{se}- and Y_{se}-axes of the solar ecliptic coordinate system are measured in earth radii, R_e.

measurement. Each of the three sections of Figure 2 represents the angular response of the cup operating in a given energy channel (labeled, respectively, by P95–235 eV, P220–640 eV, P560–2000 eV). The abscissa represents the scan angle, β, which is the angle between the normal to the collector plate and the plane containing the sun and the spin axis of the satellite. Because the cup normal is at right angles to the spin axis, $\beta=\omega t$, where ω is angular spin frequency of the satellite. The ordinate in Figure 2 represents (on a logarithmic scale) the electric current at the collector plate due to positive ions which, if the ions are protons normally incident upon the collector, have energies in the indicated intervals (P95–235 eV in the top figure, etc.) The crosses indicate actual measurements corrected for various spurious effects, such as the photo-effect, etc.

The solid curves are computed in the following way: (1) First the *response function* of the detector is constructed from its geometry and mode of operation. This function represents essentially that portion of the sensitive area of the collector plate that would record the electric current generated by a broad, parallel, monoenergetic beam of positive ions entering the cup at a given angle. (2) A study was made for the proper choice of the distribution function of positive ions in the 6-dimensional phase space. Since there are no reasons *a priori* for solar-wind ions (mostly protons) to have a Maxwell-Boltzmann distribution, various shapes were assumed, some exhibiting suprathermal tails and some varied degrees of 'thermal' anisotropies, and the effects of the detailed structure on the response of the cup investigated. (3) The final step required the proper folding of the cup response function with the flux densities of

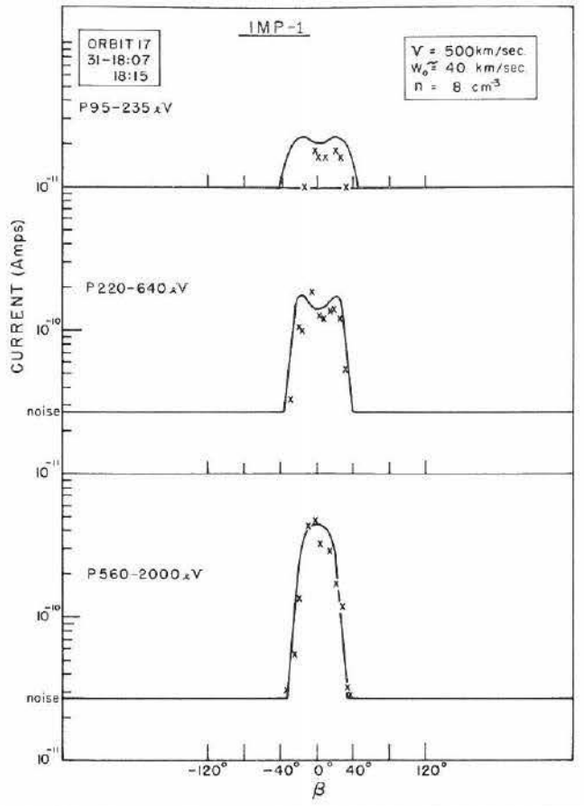

Fig. 2. An example of electric currents measured by the M.I.T. detector in the interplanetary region. The IMP-1 orbit number, the day and the duration of the observation are indicated in the upper left-hand corner. Each of the three graphs corresponds to a given energy channel for positive ions; the numbers: 95–235, 220–640, 560–2000 (eV) indicate respectively the lower and upper energy bounds of these channels. The crosses indicate the measured values of the current (in amps) corrected for the photoeffect. The solid curves represent the currents computed for Maxwellian proton distributions characterized by the parameters given in the upper right-hand corner. The abscissa of each graph represents the so-called scan angle, β, defined in the text.

positive ions corresponding to a particular distribution function and computing (on digital computers) the resulting electric current for each energy channel. Because most of the positive ion data gave relative energies (referred to the maximum of the distribution function) that fell within the three above-quoted energy intervals, and because of the broadness of the acceptance angle of the cup (1 steradian) and the broadness of adjacent energy channels, it was found that no definite conclusion could be drawn on the non-Maxwellian character of the solar-wind ions. The solid lines shown in Figure 2 correspond to the simple *ad hoc* assumption that the protons have a Maxwellian distribution in the frame of reference moving with the plasma.

The best fit of the computed curves with experimental points was achieved by appropriate variation of three 'free' parameters: the plasma density, n, the wind bulk velocity, V, and the 'thermal' speed, $w_0 = \sqrt{2kT/m_p}$. (T is the temperature and m_p the proton mass.) The 'best set' of parameters that gives the fit shown in Figure 2 is specified in the upper right-hand corner of the figure.

At this point, it is important to stress that the numerical values for n and V obtained by the procedure outlined above are quite insensitive to the detailed structure of the distribution function; a conservative estimate of the relative error that may be assigned to n and V is less than 20% and 10%, respectively. The analysis showed that the interplanetary region is characterized by a highly supersonic flow ($V \gg w_0$). However, a reliable determination of w_0 was not possible and errors as large as a factor of two must be allowed when values of w_0 are quoted. This uncertainty implies that considerable (but not excessive) anisotropy could have been present and undetected. (By anisotropy we mean here the inequality of the parallel and perpendicular

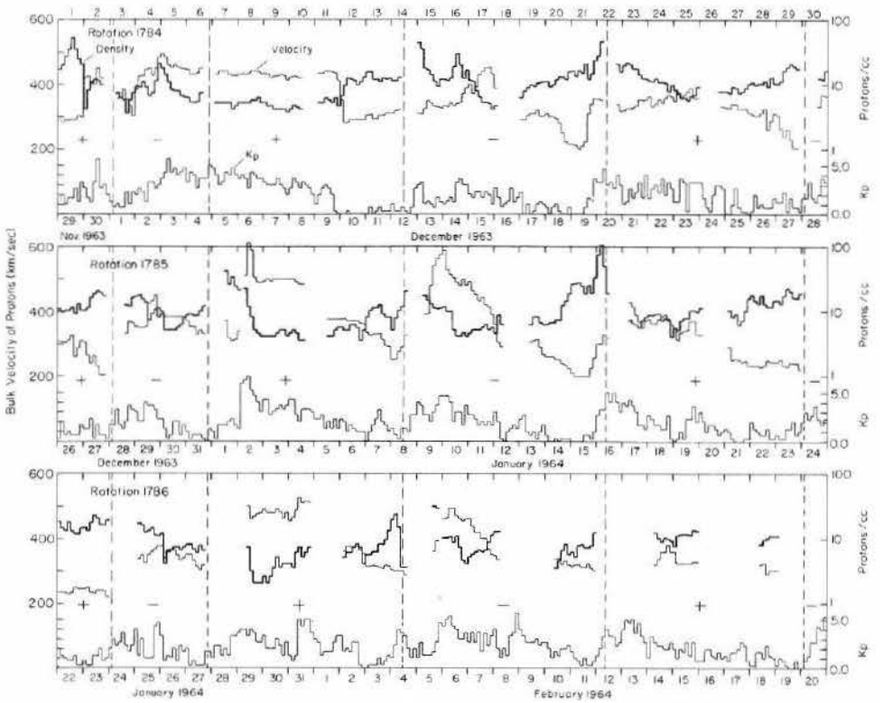

Fig. 3. The three-hour averages of the solar-wind velocity (upper light curves) and the proton number density (heavy curves) under interplanetary conditions (outside the bow shock) plotted *vs.* time (in days) for the period of 3 solar rotations: No. 1784, 1785 and 1786. The lower light curves represent the K_p index. The sections bounded by the dashed vertical lines and labeled alternately by '+' and '−' indicate the polarity of the interplanetary magnetic field.

components of the thermal ion velocity with respect to the local direction of the magnetic field.)

One 'complete' measurement of the type shown in Figure 2 requires a certain amount of time. In the case of IMP-1 the time interval is 5.5 min, and in a period of 80 days one accumulates a large number of data samples. Two persons were directly involved in the successful completion of the laborious and time-consuming analysis of the data: Dr. G. Moreno and Dr. L. Pai. We especially owe a profound debt of gratitude to the late Dr. Pai for bringing this project to fruition. His diligence and expertise cannot be overstated.

Figure 3 shows the summary of the interplanetary data reduced by Dr. Pai: the abscissa represents the time, with numbers indicating the day of a given month (from Nov. 29 through Feb. 20, 1964). The ordinate represents three physical quantities simultaneously: the heavy curve (with its logarithmic scale on the right) gives the 3-hour average of the number density of protons. The light upper curve (with its linear scale on the left) gives the 3-hour average of the solar-wind velocity (the stream or bulk velocity of protons). The lower curve (with its scale on the right) is the K_p index. The entire record was split into three separate rows, each covering one solar rotation (the rotation numbers are 1784, 1785 and 1786 and are indicated at the left upper corner of each row). The vertical dashed lines separate the periods of a given polarity of the interplanetary magnetic field; the symbols '+', '−', indicate the sign of this

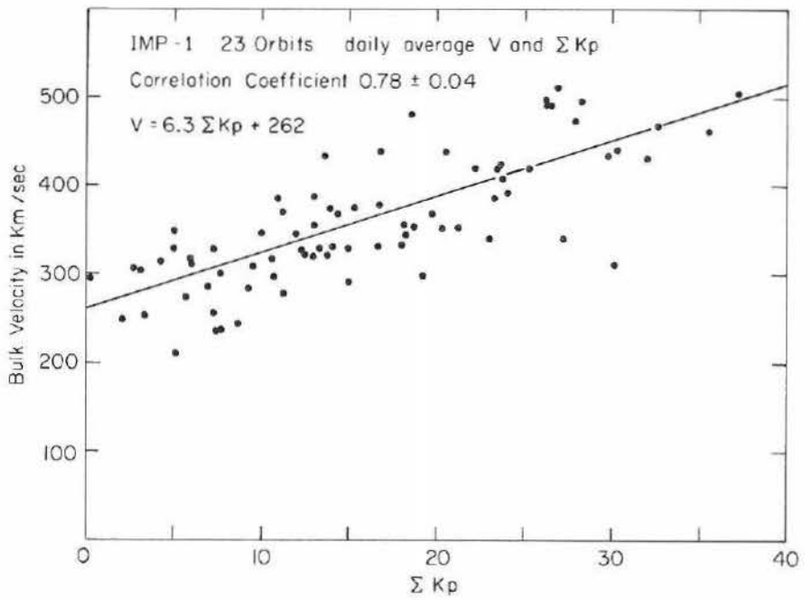

Fig. 4. The daily averages of the solar-wind velocity measured outside the bow shock during the period of the first 23 orbits of IMP-1 plotted *vs.* the daily sum of the K_p index.

polarity as determined by Drs. Ness and Wilcox on the same satellite (WILCOX and NESS, 1965).

If one examines the same polarity sector recurring after each solar rotation (say, the negative sector passing the satellite during the three successive periods of Dec. 12–20, Jan 8–16, and Feb. 4–12) one notices a rather definite tendency for the temporal behavior of a given physical quantity to reproduce itself, at least in a semi-quantitative manner. This tendency seems to be particularly pronounced for the proton density. The density is one order of magnitude higher (up to 100 protons/cm^3) during the days containing the reversal of magnetic polarity than it is near the central portion of the sector (typically 5 protons/cm^3). Because the 80-day period under consideration refers to a remarkably quiet sun, it is plausible to interpret the data as exhibiting a nearly stationary azimuthal density profile when viewed by an observer co-rotating with the sun. In this frame of reference, one would thus witness only long-time scale changes (on the order of months) of the average solar-wind parameters; one would then be tempted to correlate such changes with the gradual growth and decay of large-scale M-regions on the solar surface.

The K_p index shown in Figure 3 is seen to be quite low, as expected for a quiet sun. Following the procedure originated by Snyder, Neugebauer, and Rao on Mariner-2 (SNYDER *et al.*, 1963) Dr. Pai correlated the K_p index with the solar-wind velocity. The result is shown in Figure 4. When one plots the daily average of V vs. the daily sum of K_p, a linear relationship is found. However, the scatter of points is considerable and, consequently, the correlation is not as good as suggested by Mariner-2 results. In addition, the numerical coefficients relating V and K_p quoted in the upper left-hand corner of the graph are different from those on Mariner-2.

Figure 5 shows two histograms for the occurrence number of the observed values of the wind velocity and proton density. The intervals chosen for each column are 20 km/sec for the velocity and 1 proton/cm^3 for the density. The value occurring most often for the velocity during the IMP-1 period is about 330 km/sec, while the mean value is somewhat higher, about 360 km/sec. The distribution of the density values is more irregular, favoring higher values. The most frequently occurring and the mean density are, respectively, 4 and 7 protons/cm^3. Also, (1) the speed of the solar wind never decreased below 180 km/sec and (2), on 15 occasions, out of the total of 495 3-hour averages, the proton density exceeded the value of 28 cm^{-3}.

The obvious conclusion that one may draw from these histograms is that, even under extremely quiet solar conditions, the spread of the numerical values of observed plasma parameters is considerable. This variability makes a comparison between the theory and the experiment very difficult. Let us elaborate on this point in more detail.

All observations show invariably that at a certain distance from the earth the properties of the interplanetary plasma undergo a very sudden change. The locus of all points where this happens seems to form a rather well defined surface. The trace of this surface in the ecliptic plane is shown in Figure 1 and is labeled 'shock'.* The

* The curve shown in Figure 1 represents the *mean* position of the bow shock. The overall motions and the oscillations of the shock will be discussed later.

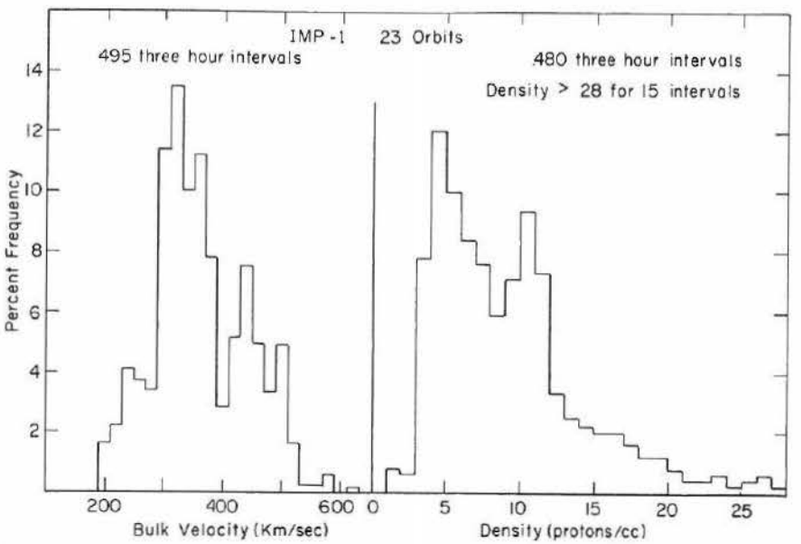

Fig. 5. Histograms of the 3-hour averages of the solar-wind velocity and number density compiled for the first 23 orbits of IMP-1 outside the bow shock.

immediate question is: Is the term shock justifiable in the fluid-dynamical sense? In other words, is it really a shock that occurs in the sense that all Rankine-Hugoniot relations are satisfied with a unique choice of parameters entering the problem (e.g., one value for the specific heat ratio γ)? Qualitative inspection of the data makes it very tempting to answer this question in the affirmative. First, *all* observed plasma parameters undergo a sudden change: the proton density, the magnitude and the direction of the wind velocity, and the proton temperature. Secondly, the changes are so sudden that the upper limit for the thickness of the transition layer separating the interplanetary regime from the magnetosheath is much smaller than 1 earth radius. Hence, in a macroscopic description of the plasma, the 'bow-shock surface' may be treated as a surface of discontinuity.

For making a quantitative test of the fluid description, the difficulty lies in the time required (at least 11 min) to accumulate a physically useful sample of data, one for each side of the bow shock. With one satellite, one cannot compare *simultaneously* the physical quantities determined just ahead of the shock with those just behind the shock. Even under favorable experimental conditions these samples will be separated by about 22 min. (This is a long time when one considers structured streams of plasma passing the satellite. For example, it takes only about 5 min for a magnetic tube of force, co-rotating with the sun, to sweep across the entire magnetosphere.) Since the plasma parameters observed well outside the bow shock often change appreciably within such time intervals, we have no justification in assuming that the pair of data samples on both sides of the bow shock belong to the same uniform plasma

stream. This circumstance renders a detailed local test of Rankine-Hugoniot relations almost impossible. In spite of this difficulty, we have carried out the program of the quantitative evaluation of physical parameters just behind the shock. We have done this in the hope that, by accumulating the data from all shock traversals, we shall be able to make statistically significant statements about the behavior of the 'grand-scale' averages of plasma parameters (each average referring to a large portion of the morning side of the magnetosheath).

As in the foregoing discussion of the data from the interplanetary regime, let us first describe in some detail the method of analysis of one 'full measurement' in the magnetosheath. Figure 6 shows a sample of one such measurement. The figure contains four separate graphs, each referring to a given positive energy channel. The abscissas and the ordinates have the same meaning as in Figure 2. The crosses indicate

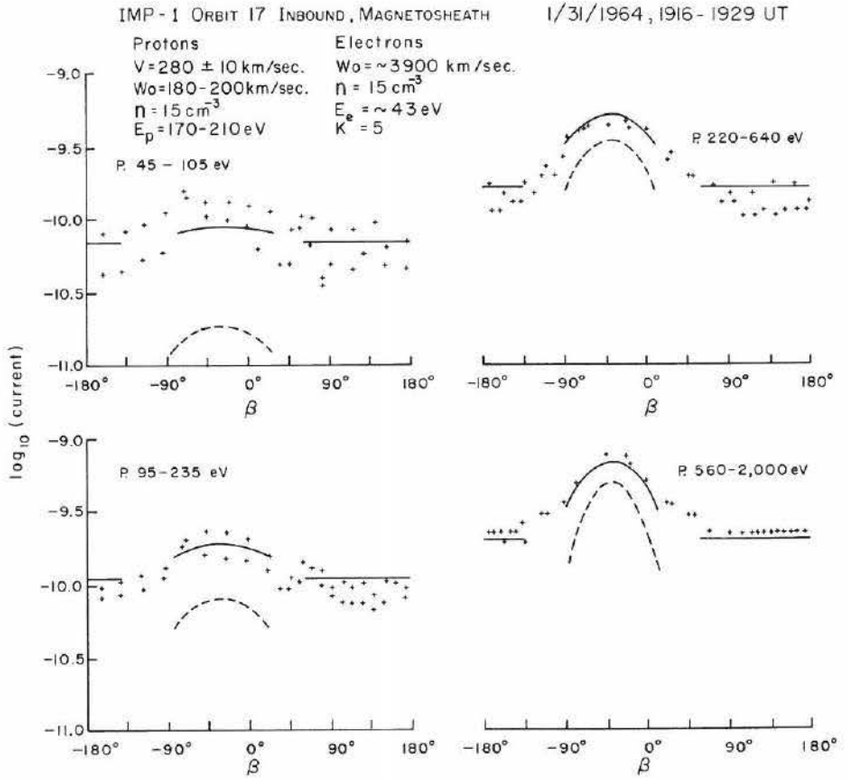

Fig. 6. An example of electric currents measured by the M.I.T. detector in the magnetosheath in 4 different energy channels for positive ions. The abscissas, ordinates and crosses have the same meaning as in Figure 2. The dashed curves indicate the computed currents due to protons alone. The solid curves represent the computed currents due to protons and the electron 'leakage'. The numbers used for the computation of these curves are indicated in the upper left-hand corner.

the actual current measurements. However, the interpretation of the currents is more complex than before. After a series of rather involved *post-factum* investigations, we now know that the currents measured in the magnetosheath by the M.I.T. detector on IMP-1 represent a superposition of two distinct contributions: (1) a contribution from positive ions in the proper energy range as predicted by the design of the instrument and (2) an *a priori* unexpected contribution from an isotropic background of heated plasma electrons.*

The dashed curves in Figure 6 indicate the computed contributions of protons under the assumption that the protons are Maxwellian in their own frame of reference and that the macroscopic parameters describing these protons fall into the range indicated by the values listed at the upper left-hand corner of the figure. The solid curves represent the computed sum of proton and electron contributions. The electric currents due to electrons (the horizontal portions of the solid curves) have been computed under the assumption that the electron speed distribution in the satellite frame of reference is of the form:

$$f_e v^2 \, dv = \text{const} \, \frac{v^2 \, dv}{\left(1 + \frac{v^2}{\kappa w_0^2}\right)^{\kappa+1}}$$

where v is the actual speed, w_0 is the most probable speed of electrons, and κ is a 'free' parameter whose value is a measure of the departure of the distribution from its Maxwellian character (letting κ approach infinity leads to the Maxwellian distribution). We shall not go into the reasons for this choice except to mention that it seems to be justifiable empirically on the basis of other independent observations. The electron parameters used to obtain the resulting curves in Figure 6 are indicated next to the proton parameters. Note that, in an attempt to reproduce the observed results by the 'best-fit' procedures discussed previously, one has now five independent parameters: n, V, w_0 for protons, w_0 for electrons, and κ. (The direction of the wind velocity is determined separately from the position of the maximum in any of the four channels.)

This five-fold freedom is far exceeded by the amount of data shown in the figure. Thus the rather fair agreement between the observations and the computations supports, at least roughly, the reasonable nature of the underlying assumptions.

* The detector was so designed that when operative on a positive modulating voltage, it could have been considered under a wide variety of conditions as insensitive to the electron background. However, the inadvertent choice of negative voltage on the suppressor grid of − 36 volts on IMP-1 made it possible for a small fraction (up to a few percent) of the collected electrons with energies comparable to or exceeding 36 eV to be modulated *via* slight changes of the effective size of the collector. This spurious effect can be shown by detailed computations of 'allowed and forbidden' trajectories of the incoming electrons to be most pronounced when the mean energy of the isotropic electrons lies in the neighborhood of 40–50 eV. It just so happens that the interplanetary electrons undergo heating processes behind the shock that lead to energies of this order of magnitude. Thus the effect turns out to be more serious than anticipated. (Changing the suppressor voltage to substantially lower values on subsequent M.I.T. detectors removed the effect completely.) Note that if the electrons were heated up to considerably higher energies, as had been speculated on theoretical grounds, the 'electron leakage' would have been hardly noticeable.

This statement should not, however, be interpreted to imply that the protons have a Maxwellian distribution in the magnetosheath. A certain degree of thermal anisotropy and a 'suprathermal tail' can well be present, but the detector is too 'integral' in its response to resolve this point unambiguously. Again, as in the interplanetary regime, one can verify by detailed computer 'experiments' that the 'best-fit' values of n and V are quite insensitive to the details of the assumed fine structure of the distribution functions. The accuracy with which we can determine n is about the same in both regions. The errors in V are now substantially larger than those quoted previously; this is primarily due to partial 'swamping' of the low-energy channels by the electron leakage. No fixed percentage error can be attached to V now. All one can say, is that the error increases with decreasing V (being about 10% at 300 km/sec) and that the determination of V below 100 km/sec becomes quite unreliable. On the other hand, the determination of w_0 is now improved in comparison with that in the interplanetary region; this is so because the observed values of w_0 turn out to be substantially higher (subsonic and transonic flow).

Figure 7 shows the results of the search for the location of the magnetosheath.

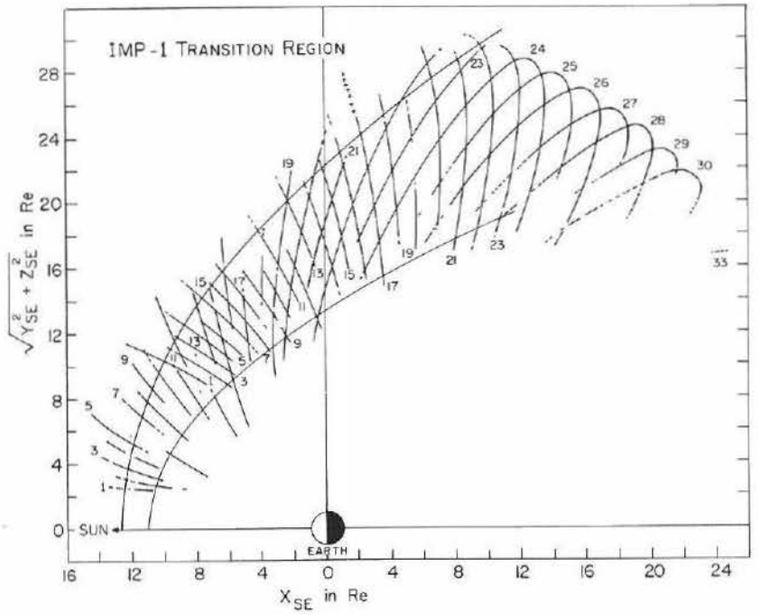

Fig. 7. The boundaries of the magnetosheath (or the 'transition' region) as determined by the M.I.T. detector on IMP-1. Each solid segment of the curves labeled 1 through 30 indicates that portion of the projected orbit where the solar wind plasma exhibits the behavior characteristic of the magnetosheath. The two curves crossing the sun–earth line represent the 'mean' positions of the bow shock and the magnetopause, respectively, obtained by the rms fitting procedures. The coordinates are the same as in Figure 1.

Each curve accompanied by an integer indicates the ecliptic projection of that portion of a given orbit (from 1 to 30) that contained plasma measurements of the type shown in Figure 6. All measurements during the time intervals corresponding to the solid curves had the following characteristics in common: (1) the wind was diverted from its original (essentially solar) direction; (2) the magnitude of the stream velocity of protons was reduced in comparison to that in the interplanetary region; (3) the thermal speed of protons was correspondingly enhanced; and (4) substantial fluxes of isotropic electrons with energies greater than about 20 eV were readily detectable at all times.

At distances further from the earth than the projected curves of Figure 7, we always found plasma in the condition characterized by Figure 2; conversely, at distances closer to the earth, we found no measurable flux of positive ions. Thus the inner ends of the curves in Figure 7 indicate the position of the magnetopause. It is evident from the figure that it is not possible to draw a smooth curve through either inner or outer ends of the drawn segments of the orbits. In view of the observed variations of the dynamic pressure of the solar wind far away from the magnetosphere, and in view of the fact that the individual segments of a given orbit refer to widely different time intervals, it is clear that the lack of smoothness does not imply ragged, stationary surfaces of the bow shock and the magnetopause, but rather a variable position of

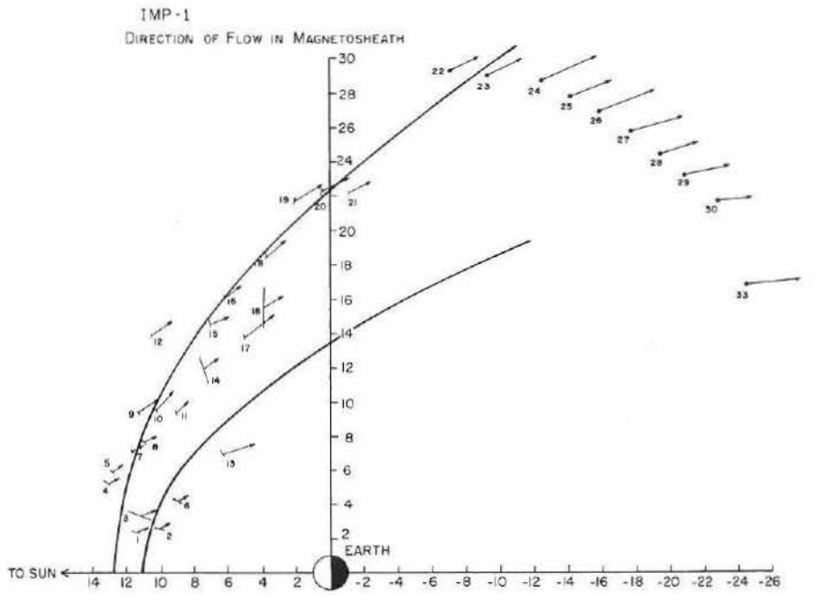

Fig. 8. A 'map' showing the directions of the streaming velocity of positive ions observed on IMP-1 under the conditions characteristic of the magnetosheath. The number and stub attached to each vector indicate the inbound portion of the orbit used for the shown sample. The velocity vectors are rotated into a common plane as explained in the text. The coordinates are the same as in Figure 1.

TABLE I

IMP-1 Solar-Wind Data in Regions I and II near the Shock Transition

Orbit	Time (min)		Density n (cm^{-3})		V (km/sec)		Proton Thermal Energy (eV)		Electron Thermal Energy (eV)	
	I	II	I	II	I	II	I	II	I	II
1 IN	54	20	9	12	410 ± 10	100 ± 20	≲ 19	≈ 210	57	
2 IN	10	21	6	11	440 ± 10	100 ± 10	≲ 8	≲ 105	64	
3 IN	32	74	4	10	415 ± 10	160 ± 20	≲ 19	105–170	51	
4 IN	21	26	12	22	320 ± 10	100 ± 20	≲ 19	35–80	50	
5 IN	77	42	5	14	390 ± 10	100 ± 20	13–19	≲ 105	43	
6 IN	19	19	48	54	330 ± 10	100 ± 20	≲ 8	≲ 80	60	
7 IN	41	11	10	13	370 ± 25	100 ± 30	19–52	≲ 105	65	
8 IN	20	22	20	30	210 ± 10	125 ± 20	≲ 8	≲ 55	43	
9 IN	26	20	12	14	340 ± 10	200 ± 20	8–19	≈ 35	53	
10 IN	55	20	4	10	485 ± 15	200 ± 20	≲ 19	≲ 255	45	
11 IN	73	20	20	40	325 ± 20	125 ± 20	≲ 19	135–170	33	
12 IN	22	11	6	12	290 ± 10	200 ± 20	≲ 33	135–170	55	
13 IN	30	12	18	33	320 ± 20	280 ± 10	≲ 33	≲ 255	71	
14 IN	33	84	11	13	325 ± 20	150 ± 10	≲ 33	80–105	55	
15 IN	44	33	15	64	240 ± 10	160 ± 10	8–13	≈ 35	30	
16 IN	09	22	6	28	325 ± 20	160 ± 10	8–19	105–135	15	
17 IN	11	19	6	15	525 ± 10	280 ± 10	≲ 8	170–210	43	
18 IN	23	8	2	10	320 ± 10	270 ± 10	≲ 19	90–120	65	
19 IN	24	31	13	22	350 ± 10	275 ± 10	13–19	55–80	30	
20 IN	85	43	12	35	300 ± 10	240 ± 10	13–19	50–60	19	
21 IN	81	22	11	30	325 ± 10	190 ± 10	≲ 19	105–135	24	
22 IN	19	19	9	27	310 ± 10	250 ± 10	≲ 8	35–55	16	
23 IN	22	21	10	21	325 ± 10	285 ± 10	11–16	25–45	19	

these surfaces. We shall demonstrate the validity of this interpretation below in discussing the issue of multiple transitions.

We are now ready to discuss the results of the quantitative analysis of data in the magnetosheath. Let us begin with the spatial distribution of the directions of the solar-wind velocity behind the bow shock. Figure 8 shows the summary of 33 samples taken during time intervals (indicated by the length of the stub attached to the base of each vector) when plasma was in the magnetosheath; each vector corresponds to an inbound portion of a different orbit as labeled. The vectors indicate the plasma flow directions rotated into a common plane containing the plasma velocity and the sun–earth line. The representation is meaningful if one assumes that the wind flow pattern has axial symmetry about the line passing through the earth and parallel to the wind velocity in the interplanetary regime (the average aberration angle due to the orbital motion of the earth is only about 5°). We have made this assumption throughout our analysis; one can show by plausible arguments that it is justifiable if the data refer to points in space not too far from the ecliptic plane. (This is one reason why we only used the *inbound* portions of the satellite trajectories.) With the assumption of axial symmetry it is relatively easy to determine the flow direction from the known aspects of the detector motion (location, spin, etc.) and the value of the scan angle β at the current maximum (see Figure 6).

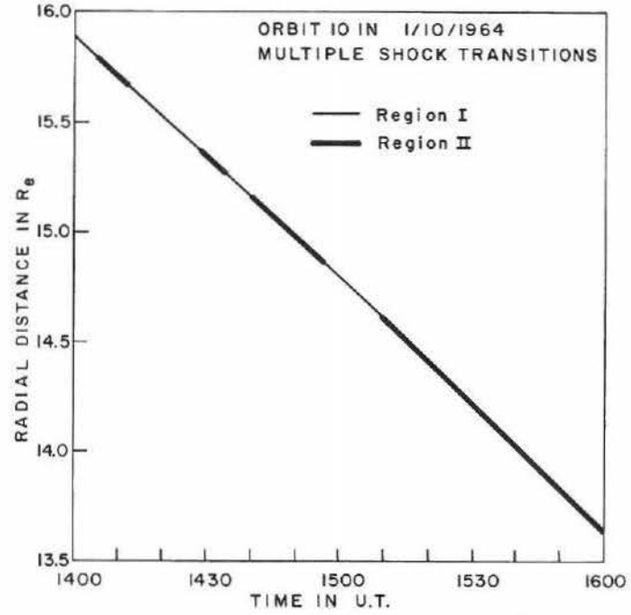

Fig. 9. An example of multiple transitions. The ordinate is the radial distance of IMP-1 from the earth's center, shown as a function of time during the inbound portion of the 10th orbit flight. The heavier segments of the curve indicate plasma with magnetosheath characteristics; the lighter portions of the curve refer to plasma with characteristics of the interplanetary regime.

TABLE II

IMP-1 Multiple Shock Transitions

Transition Number	Time in U.T. day	(year) hr.	Average Shock Position X_{se} (R_e)	Y_{se} (R_e)	Z_{se} (R_e)	R (R_e)	# of Crossings N_c	Total Time $(\Delta T)_{tot}$ (min)	Total Distance $(\Delta R)_{tot}$ (R_e)	$\bar{U} = \frac{(\Delta R)_{tot}}{(\Delta T)_{tot}} N_c$ (km/sec)
		1963								
1 IN	334	1735	12.69	− 1.58	2.06	13.01	7	54	1.16	16
2 IN	338	1505	12.26	− 2.18	2.15	12.64	7	60	1.29	16
3 IN	342	1123	13.02	− 3.52	2.09	13.64	5	84	1.73	11
4 IN	346	0855	12.58	− 4.39	2.21	13.54	3	95	1.94	7
5 IN	350	0355	14.50	− 6.84	2.01	16.18	1	–	–	–
6 IN	354	0522	9.79	− 4.00	2.54	10.89	1	–	–	–
7 IN	357	2338	12.28	− 7.46	2.29	14.61	3	24	0.67	10
8 IN	361	2115	11.54	− 8.01	2.38	14.22	3	28	0.49	5
9 IN	365	1705	11.96	−10.02	2.25	15.78	1	–	–	–
		1964								
10 IN	4	1440	10.95	−10.28	2.33	15.21	7	64	1.19	12
11 IN	8	1315	9.41	− 9.67	2.58	13.76	3	12	0.20	5
12 IN	12	0535	10.88	−15.21	2.01	18.85	3	136	1.97	5
13 IN	16	0850	7.50	− 9.10	2.81	12.13	5	122	2.64	11
14 IN	20	0210	8.14	−14.19	2.41	16.56	1	–	–	–
15 IN	24	0010	7.01	−13.96	2.56	15.84	3	66	1.14	6
16 IN	27	1828	6.37	−17.30	2.19	18.58	5	74	1.12	8
17 IN	31	1838	5.07	−14.37	2.64	15.49	3	15	0.27	6
18 IN	35	1310	3.84	−17.62	2.35	18.19	5	133	1.97	8
19 IN	39	0530	2.06	−21.99	1.66	22.17	1	–	–	–
20 IN	42	2335	− 0.03	−23.98	1.17	24.04	5	71	0.69	5
21 IN	46	2245	− 1.27	−22.67	1.54	22.79	3	30	0.33	4
22 IN	50	0140	− 7.17	−29.42	−1.71	30.36	3	78	0.27	1
23 IN	53	2056	− 9.49	−29.11	−1.99	30.71	1	–	–	–
										$\bar{U}_{av} = 8$

TABLE III

IMP-1 Multiple Shock Transitions

Transition Number	Time in U.T. day	(year) hr.	Average Shock Position X_{se} (R_e)	Y_{se} (R_e)	Z_{se} (R_e)	R (R_e)	# of Crossings N_c	Total Time $(\Delta T)_{tot}$ (min)	Total Distance $(\Delta R)_{tot}$ (R_e)	$\bar{U} = \frac{(\Delta R)_{tot}}{(\Delta T)_{tot}} N_c$ (km/sec)
		1963								
1 OUT	331	1228	12.35	− 9.65	−6.23	16.88	1	–	–	–
2 OUT	335	0750	9.57	− 9.38	−5.84	14.64	3	16	0.38	8
3 OUT	339	0536	9.30	−10.37	−5.92	15.15	1	–	–	–
4 OUT	343	0330	9.31	−11.52	−6.06	16.01	5	73	1.23	9
5 OUT	346	2355	7.69	−11.32	−5.91	14.92	1	–	–	–
6 OUT	350	2355	8.81	−13.78	−6.32	17.56	3	12	0.16	4
7 OUT	354	1955	6.98	−13.56	−6.16	16.47	3	28	0.51	6
8 OUT	358	1810	6.77	−14.84	−6.29	17.51	1	–	–	–
9 OUT	362	1442	5.20	−14.57	−6.16	16.67	1	–	–	–
		1964								
10 OUT	1	1135	3.90	−14.62	−6.11	16.33	1	–	–	–
11 OUT	5	1140	4.34	−17.53	−6.43	19.18	7	80	1.15	11
12 OUT	9	0700	2.40	−16.00	−6.26	17.37	1	–	–	–
13 OUT	13	0940	2.98	−20.46	−6.59	21.72	3	28	0.36	4
14 OUT	17	0555	1.28	−20.00	−6.57	21.12	3	52	0.69	4
15 OUT	21	0520	0.47	−21.75	−6.58	22.76	1	–	–	–
16 OUT	25	0530	− 0.48	−23.62	−6.50	24.53	5	147	1.41	5
17 OUT	29	–	–	–	–	–	–	–	–	–
18 OUT	33	0235	− 3.51	−24.99	−6.37	26.05	5	194	1.59	4
19 OUT	36	2020	− 5.28	−22.61	−6.50	24.14	11	558	5.22	11
20 OUT	41	0930	− 5.96	−29.16	−5.15	30.24	1	–	–	–
21 OUT	45	0700	− 7.96	−28.81	−5.09	30.35	1	–	–	–
22 OUT	49	1345	− 8.99	−29.86	−3.69	31.44	9	392	0.21	1
23 OUT	53	1230	−10.79	−29.29	−3.40	31.44	1	–	–	–
										$\bar{U}_{av} = 6$

We believe Figure 8 demonstrates rather convincingly a systematic diversion of the proton flow from the solar direction. Detailed numerical checks verify this conclusion even further: they show that the directional pattern obtained is totally consistent with the flow pattern of an ordinary fluid, streaming with hypersonic velocity ahead of the bow wave past a blunt body of the shape of the magnetosphere.

In Figure 8, the length of the vectors drawn indicates the observed magnitude of the streaming velocity behind the bow shock. One may notice the gradual average increase in V as one proceeds past the sonic surface. Further back, toward the magnetospheric tail (orbits 19 through 30) the wind speed regains again its high pre-shock value, as expected on the ordinary fluid picture.

Turning now to the scalar plasma parameters, Table I gives the summary of the solar wind data taken on the inbound portion of each orbit in the immediate vicinity of the bow shock. The columns labeled by (I) and (II) refer to the interplanetary region and the magnetosheath, respectively. The first column identifies the inbound orbit to which the data refer; the next two columns indicate, in min., the duration of the time intervals of the analyzed data samples on both sides of the shock. The following three pairs of columns give the numerical values of the proton number density (in cm^{-3}), the wind velocity (the bulk proton velocity in km/sec) and the 'thermal energy' (in eV). The final column gives the 'thermal energy' (in eV) of the magnetosheath electrons, $kT_e = \frac{1}{2} m_e w_{0,e}^2$, as determined from their leakage in positive energy channels. Concentrating our attention on columns referring to region I, we note that the plasma parameters (especially the density) change considerably from orbit to orbit, making any assumption of a steady character of the plasma flow across the bow shock quite indefensible. Nevertheless, we note that the post-shock value of the density is always higher than the corresponding pre-shock value. As a rule, the jump amounts to a factor of 2 or 3.

The few cases for which the jump is less than two, turn out to refer to time intervals when the plasma is more disturbed than usual. Next, the velocity decreases across the shock are seen to be quite systematic. As expected from the fluid description of the plasma, the relative jumps are more pronounced closer to the subsolar region (orbits 1 through 8) than toward the dawn side of the magnetosphere (orbits 9 through 23). The most dramatic change takes place in the proton thermal energies. They jump often from low values of the order of 10 eV or less ($T_p \lesssim 10^5$ K) to high values of the order of 100 eV ($T_p \approx 10^6$ K). Because of the low fluxes (associated with the low temperatures) we were not able to detect any electrons in region I. When one makes the reasonable assumption that the electron temperature is probably not too different from that of protons in the interplanetary regime (an assumption which seems to be supported by a few sporadic, independent measurements), then one arrives at the rather surprising conclusion that the electrons are heated to a much smaller degree than protons behind the shock. The entries in the last column of Table I indicate an electron temperature of about 5×10^5 K or less.

The results in Table I that refer to protons can be shown by more detailed tests not to be in contradiction with the theoretical results obtained on the basis of a one-

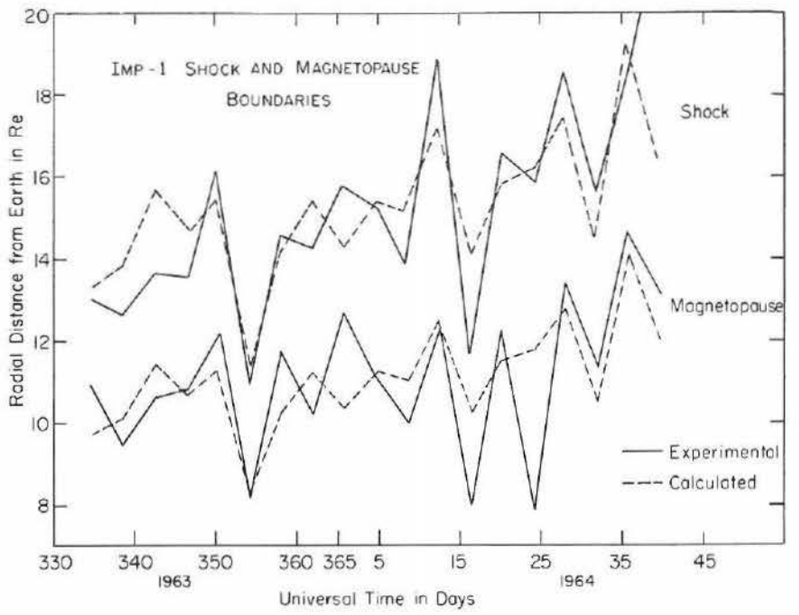

Fig. 10. The radial distances from the earth's center of the bow shock and the magnetopause at the time when IMP-1 crosses one of these boundaries, compiled for the first 19 inbound passes and averaged over the multiple transitions in each pass. The corners of the solid and dashed curves correspond to the observed and computed 'points', respectively.

fluid model description of the solar plasma in which the dynamical effects of the interplanetary magnetic field are ignored. (This latter simplification is well justified on the morning side of the magnetosphere, where the direction of the average magnetic field is rather close to the normal of the bow-shock surface. This implies, for this region, that the magnetic pressure will not suffer a substantial jump across the shock and thus will remain considerably smaller than the thermal and dynamic pressures of positive ions in the magnetosheath.) Of course, the data obtained by the M.I.T. detector on IMP-1 are too crude to allow an unambiguous determination of such parameters as the specific heat ratio, γ, which, in our opinion, should come out to be $\frac{5}{3}$.

Let us now turn our attention to a different phenomenon observed on IMP-1 in connection with the studies of the bow-shock crossings. This phenomenon has also been seen by other investigators and is usually referred to as the 'multiple shock transition'. Referring to Figure 7 we see that some portions of the satellite trajectory in the magnetosheath are drawn with several interruptions. This indicates that the detector was exposed back and forth, in an alternate sequence, to plasma under interplanetary and magnetosheath conditions. Figure 9 shows this in more detail with the example of the inward pass of orbit 10. The figure represents the radial distance of the satellite as a function of time. The heavily drawn portions of the curve refer to the time

intervals when the plasma had all the characteristics of the magnetosheath (Region II). During the remainder of the time shown on the graph the plasma exhibited all the characteristics of the interplanetary regime (Region I). We thus observed, in the case of the inbound orbit 10, seven bow-shock crossings. Tables II and III summarize the findings of such multiple transitions for the inbound and outbound segments of individual orbits, respectively. In both tables, the first seven columns, indicating respectively the orbit, the time, the average position of the bow shock and the number of multiple crossings, are self-explanatory. The next two columns, labeled by $(\Delta T)_{\text{tot}}$ and $(\Delta R)_{\text{tot}}$, give respectively the total time elapsed and the total radial distance covered by the satellite from the moment of the first transition to the moment of the last transition. One notes from these tables that the occurrence of multiple transitions is a rather persistent phenomenon (only 6 single crossings in 23 inbound passes and 11 single crossings in 22 outbound passes were observed). These findings thus suggest strongly the now familiar interpretation that the bow-shock surface is not stationary but rather is in a state of continuous oscillatory motion. The precise form of this motion cannot be deduced from this type of data alone. Nevertheless one can get a rough estimate of the radial aspect of the motion by interpreting $\frac{1}{2}(\Delta R)_{\text{tot}}$ as the amplitude and $[2(\Delta T)_{\text{tot}}/(\text{number of crossings})]$ as the period of these oscillations. Then the root-mean-square radial velocity, $\bar{U}$, associated with this motion is given by

$$\bar{U} = \frac{\pi}{2\sqrt{2}} \frac{(\Delta R)_{\text{tot}}}{(\Delta T)_{\text{tot}}} N_c \approx \frac{(\Delta R)_{\text{tot}}}{(\Delta T)_{\text{tot}}} N_c ,$$

where N_c is the total number of crossings in a given multiple transition. The quantity $\bar{U}$ is quoted in the last column of Tables II and III. Its overall average comes out to be ≈ 7 km/sec.

To conclude our review of the IMP-1 measurements obtained by the M.I.T. Faraday Cup, we should discuss briefly the results pertaining to the relative radial distances of the bow shock and the magnetopause. Figure 10 shows these distances as functions of time for the first 19 orbits. Each corner of the two solid, saw-tooth shaped curves represents the *observed average* radial distance of the bow shock or the magnetopause on a given pass. One sees a definite correlation between these two curves. Both zig-zag patterns follow each other with remarkable consistency. The dashed curves are the results of numerical calculations based on the following, simple model: Using the classical Chapman-Ferraro arguments, one assumes that the distance of the subsolar point on the magnetopause (the stagnation point), R_s, is completely determined by the balance between the dynamic pressure of the solar wind under pre-shock conditions and the pressure of the compressed magnetic dipole at the stagnation point, B_s, i.e.,

$$n m_p V^2 = \xi \frac{B_s^2}{8\pi} = \frac{\xi}{2\pi} \frac{M^2}{R_s^6}$$

where ξ is a dimensionless numerical factor of the order of unity and M is the magnetic moment of the earth's dipole. One can estimate the value of ξ from the data

and modify the above formula to apply not only to the sun–earth line but also to other points on the morning-side portion of the magnetopause (with replacement of V by the component of bulk velocity normal to the bow shock surface, etc.). Assuming that ξ stays the same for all points, one then can derive a formula that relates uniquely the radial distance of a given point on the magnetopause with the dynamic pressure of the solar wind at 'infinity'. By introducing the scaling factors relating the observed average shape of the magnetopause to that of the bow shock, one can also construct similar formulas for the bow-shock distances. One can see from Figure 10 that the computed curves follow the observed ones fairly well. This lends strong support to the familiar theoretical argument that the dynamical pressure of the freely streaming solar wind plays a controlling role in determining the shape and the size of the magnetosphere.

In an attempt to summarize in one sentence the most significant conclusion of our investigations, I would be inclined to say this: *A macroscopic fluid model may be considered as adequate* for the purpose of a description of the gross features of the solar wind. This conclusion is not by any means self-evident. We must keep in mind that the interplanetary plasma is 'collisionless' as far as the ordinary Coulomb collisions are concerned. A presence of copious particle-wave interactions must exist to explain the bow-shock formation and other phenomena. A search for the most important mode of these interactions must continue, which we hope will meet with success in the forseeable future.

Acknowledgements

This work was supported in part by the National Aeronautics and Space Administration under grant NsG-386, and contract NAS 5-2952 (with the Goddard Space Flight Center).

References

Ness, N. F.: 1966, 'Earth's Magnetic Field: A New Look', *Science* **151**, 1041–1052.

Snyder, C. W., Neugebauer, M., and Rao, V. R.: 1963, 'The Solar Wind Velocity and its Correlation with Cosmic-Ray Variations and with Solar and Geomagnetic Activity', *J. Geophys. Res.* **68**, 6361–6370.

Wilcox, J. M. and Ness, N. F.: 1965, 'Quasi-stationary Corotating Structure in the Interplanetary Medium', *J. Geophys. Res.* **70**, 5793–5805.